A C T A A S T R O N O M I C A

Vol. 31.4 1981

On the Emission Lines from Rotating Gaseous Disks

by

J. Smak

N. Copernicus Astronomical Center, Polish Academy of Sciences Warsaw, Poland

Received June 9, 1981

ABSTRACT

Theoretical profiles are calculated for a flat, Keplerian disk with the emissivity law $f(r) \sim r^{-a}$ and including the effects of finite spectral resolution. The profiles are double peaked with the peak velocity being by about 6 percent larger than the rotational velocity $V_d \sin i$ of the outer edge of the disk. The effect of finite spectral resolution can partly explain the invisibility of doubling at low orbital inclinations. The r^{-a} emissivity law appears well applicable to disks in cataclysmic variables, with $a \cong 2$. The emissivity extends down to inner radii as small as 0.02 - 0.10 of the outer radii with no systematic difference between objects representing different types of cataclysmic variables. An extra central emission of unknown origin appears to contribute to the observed profiles in ceratin objects (SS Cyg, G61-29) making their double structure less pronounced or invisible.

1. Introduction

Emission lines originating in rotating, gaseous disks are common in close binary systems, in particular in cataclysmic variables. When the orbital inclination is close to 90° they show characteristic double profiles. It was shown earlier (Smak 1969, Huang 1972) that such a double structure is likely to be a consequence of (*i*) flat geometry and (*ii*) Keplerian rotation of the disk. In particular, it was shown (Smak 1969) — and used often in various applications — that the velocity defined by these peaks is roughly identical with the rotational velocity $V_d \sin i$ at the outer rim of the disk.

In general, in the case of a flat, Keplerian disk, the profile of the emission line is determined by the inner and outer disk radii and — assuming axial symmetry — by the density distribution $f(r)$ of the emitting atoms. Conversely, from an analysis of the observed profile one can determine the parameters of the disk. In a more special case, when the disk undergoes an eclipse, an analysis of the eclipse behaviour of the emission lines results in a determination of several important parameters of the binary system (cf. Young and Schneider 1980, 1981, Young *et al.* 1981). It can only be added that the knowledge of the disk parameters, including the shape of the density distribution function $f(r)$, is essential for studying in more detail the physical mechanisms of the emission line formation (cf. Williams 1980).

This paper presents a series of theoretical profiles, calculated for a range of parameters involved, with a particular emphasis on the effect of finite spectral resolution of the observed profiles. This will be followed by a discussion based on examples of observational data.

2. Theoretical Profiles

We assume, as is commonly done, that the disk is flat and Keplerian. We assume furthermore that there is axial symmetry and that the density distribution of the emitting atoms is given by $f(r)$. We neglect all other effects (some of them will be discussed later). Let us adopt dimensionless variables such that the radii and rotational velocities at the inner and outer edges of the disk are:

inner: r_1, and $v_1 = r_1^{-1/2}$
outer: $r_2 = 1$, and $v_2 = 1$.

The emission line profile in terms of the dimensionless radial velocity u is

$$F(u) \sim \int_{r_1}^{r_z} \frac{r^{3/2} f(r)\,\mathrm{d}r}{(1-u^2 r)^{1/2}}, \tag{1}$$

where $r_z = \min(1, u^{-2})$. (At this point it should be noted that Eq. (5) in Smak (1969) contained an error; fortunately, it did not affect major qualitative conclusions of that paper). Substituting $x = u\,r^{1/2}$ we obtain

$$F(u) \sim u^{-5} \int_{x_1}^{x_z} \frac{x^4 f(x^2/u^2)\,\mathrm{d}x}{(1-x^2)^{1/2}}, \tag{2}$$

where

$$x_z = \min(u, 1), \quad x_1 = ur_1^{1/2}. \tag{3}$$

Following preliminary evidence (Fabian *et al.* 1979, Smak 1981, Young and Schneider 1980, and others) we now assume

$$f(r) \sim r^{-a}, \tag{4}$$

where a is expected to be near 1 or 2. In this case Eq. (2) becomes

$$F(u) \sim u^{2a-5} \int_{x_1}^{x_z} \frac{x^{4-2a}\,dx}{(1-x^2)^{1/2}}. \tag{5}$$

For specific values of a the integral can be expressed analytically and we can write

$$F(u) \sim u^{2a-5}[I(a, x_z) - I(a, x_1)], \tag{6}$$

where

$$I(0, x) = -\left(\frac{x^3}{4} + \frac{3x}{8}\right)(1-x^2)^{1/2} + \frac{3}{8}\arcsin x, \tag{6a}$$

$$I(0.5, x) = \frac{1}{3}(1-x^2)^{3/2} - (1-x^2)^{1/2}, \tag{6b}$$

$$I(1, x) = -\frac{x}{2}(1-x^2)^{1/2} + \frac{1}{2}\arcsin x, \tag{6c}$$

$$I(1.5, x) = -(1-x^2)^{1/2}, \tag{6d}$$

$$I(2, x) = \arcsin x, \tag{6e}$$

$$I(2.5, x) = \ln\{[1-(1-x^2)^{1/2}]/x\}. \tag{6f}$$

Quite generally, we can conclude that with $f(r)$ given by relation (4), the shape of the profile depends only on two parameters: a and r_1.

To make the theoretical profiles comparable to the observed ones we now introduce the effect of the finite spectral resolution. We assume that in dimensionless units the resolution is Δu; in terms of the observed parameters Δu is the ratio of the instrumental resolution (expressed in velocity units) to the true rotational velocity of the outer rim of the disk. Note that until now we did not have to consider the orbital inclination i; in fact, for all cases with $i \neq 90°$, the relevant parameters should be multiplied by $\sin i$. At this point we should emphasize that, at a given instrumental resolution, Δu depends on $V_d \sin i$.

All theoretical profiles are now broadened with a Gaussian profile with FWHM $= \Delta u$. An alternative would be to use rectangular profile but it appears that the adoption of a specific broadening profile as little

effect on the final results. Finally, the resulting theoretical profiles are normalized to peak intensity = 1.

The overall result of calculations described in this Section is a three-dimensional family of normalized, dimensionless profiles: $F(u; \alpha, r_1, \Delta u)$.

3. Discussion of Theoretical Profiles

3.1. The Shapes of the Profiles.

As found earlier (Smak 1969, Huang 1972) the profiles are distinctly double. The effect of various parameters upon their shapes is illustrated in Figs. 1-3. Concerning the dependence on α and r_1 we note that — in

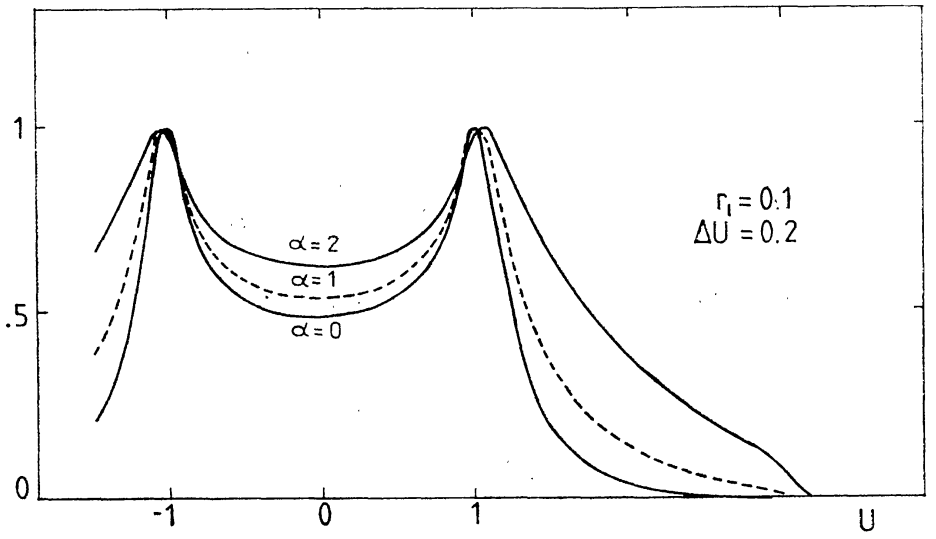

Fig. 1. Examples of theoretical profiles showing the dependence on r_1.

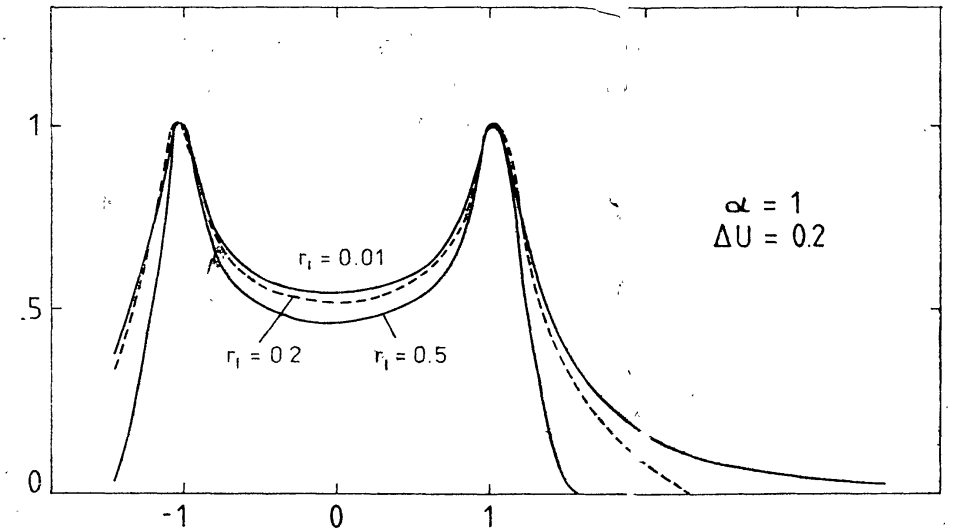

Fig. 2. Examples of theoretical profiles showing the dependence on α.

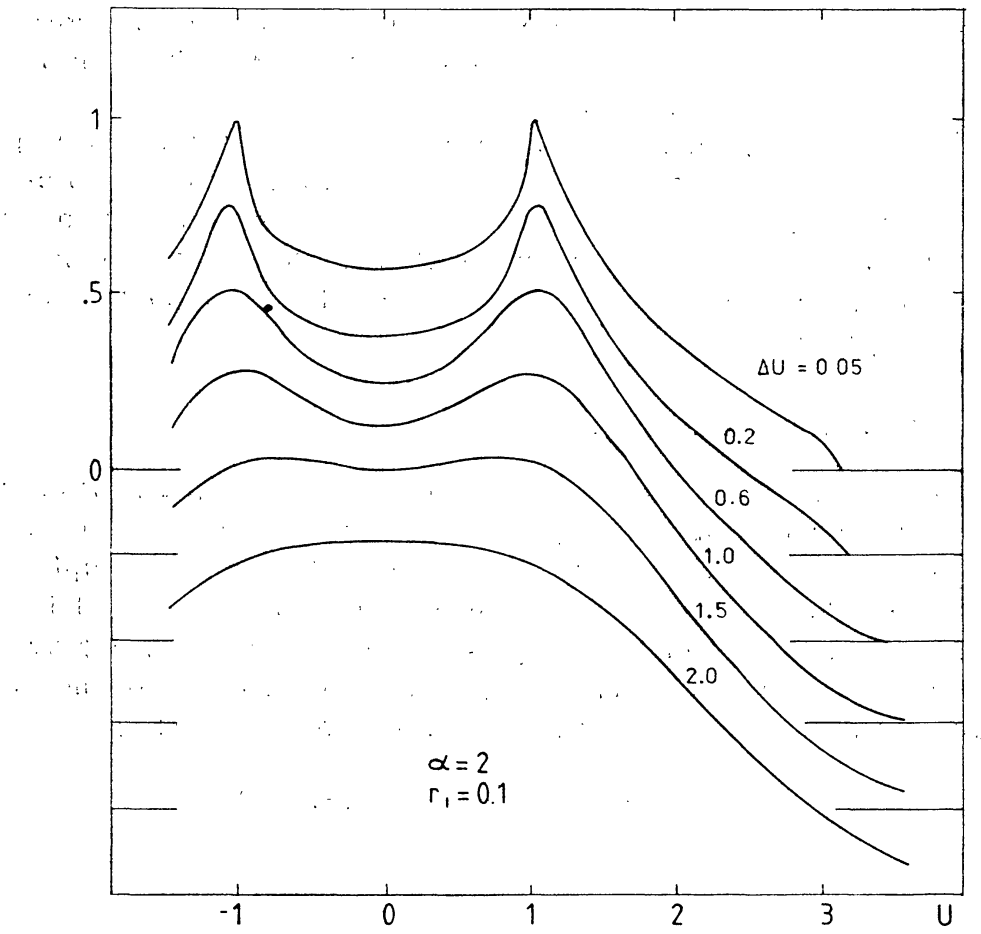

Fig. 3. Examples of theoretical profiles showing the dependence on Δu.

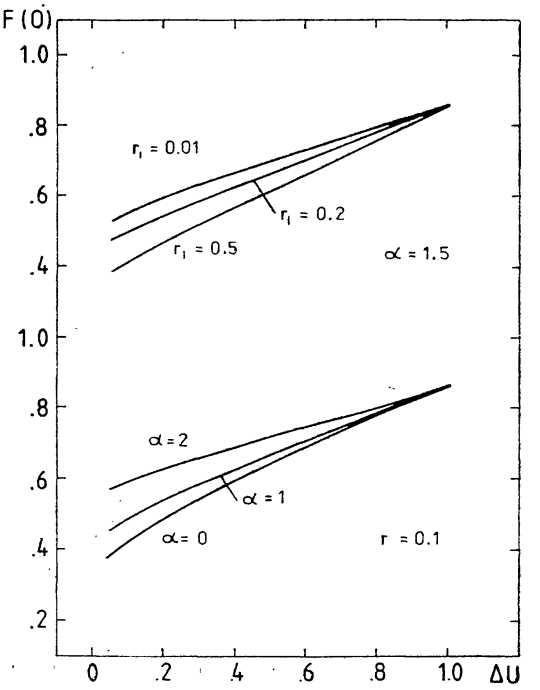

Fig. 4. Central intensity $F(0)$, normalized to peak intensity, as a function of the three parameters.

both cases (Figs. 1 and 2) — the effect is largest in the wings: increasing α or decreasing r_1 makes the wings more pronounced; the effects of α and r_1 are, however, rather different.

Concerning the dependence on Δu (Fig. 3) we note that it affects primarily the visibility of the peaks. With increasing Δu they become broader and the central depression becomes less deep. This can also be seen from Fig. 4. At $\Delta u = 1$ the central intensity $F(0)$ is only about 15 percent below the peak level, while at higher values of $\Delta u = 1.5$-2.0 the double structure disappears.

3.2. Central Intensity and Peak Velocity.

As can be seen from Fig. 4, the central intensity $F(0)$ depends primarily on Δu. Its dependence on α and r_1 is not very strong. For typical ranges of parameters: $\alpha = 1.5$-2.2, $r_1 \leqslant 0.1$ (cf. Section 4.2) we may adopt that $F(0) \cong 0.5$ for $\Delta u \leqslant 0.2$ and increases up to $F(0) \cong 0.7$ at $\Delta u = 0.6$.

The observed separation of the peaks in the double profile provides an estimate of the rotational velocity $V_d \sin i$ at the outer rim of the disk. It is obvious that the observed and true values can be related by

$$(V_d \sin i)_{\text{true}} = (V \sin i)_{\text{peak}} / u_{\max}, \qquad (7)$$

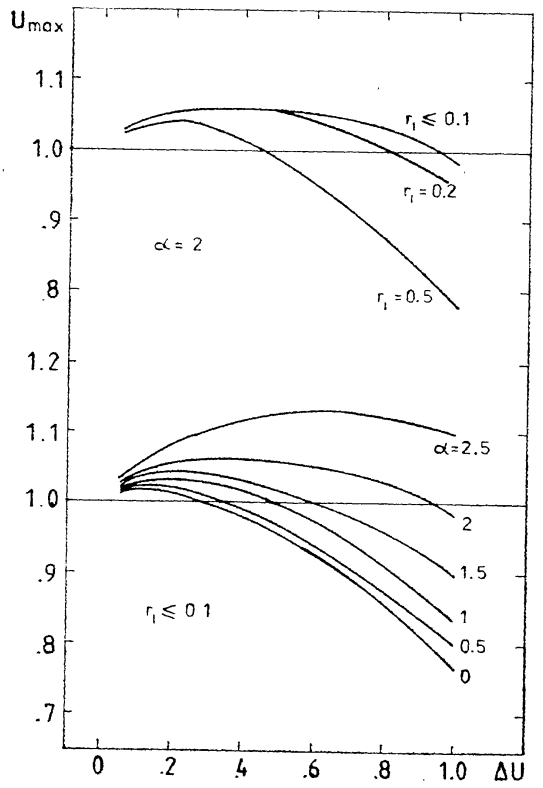

Fig. 5. Dimensionless velocity of the peak as a function of the three parameters.

where u_{max} is the dimensionless velocity of the peak; theoretical profiles give u_{max} as a function of the parameters involved. This is shown in Fig. 5 and we can see that for the applicable range of parameters (cf. Section 4.2) we may adopt

$$u_{max} = 1.05 \pm 0.05. \quad (8)$$

Thus to obtain the true value of $V_d \sin i$ one has to decrease the observed peak value by about 5 percent. It should be added, however, that unless the observed peaks are sharp the reliable determination of their position may not be a simple problem and can be a subject to systematic errors.

3.3 Half-Widths of the Profiles.

For either a theoretical or an observed profile we can introduce and measure its half-widths at specific intensity levels. Taking into account the shapes of the theoretical profiles and the observational limitations we select the three levels: 0.8, 0.4, and 0.1 (in units of the peak intensity). Thus for each theoretical profile we have in dimensionless units: $u(0.8)$, $u(0.4)$, and $u(0.1)$. Their observational equivalents (for example in km/s) will be the half-widths: $W(0.8)$, $W(0.4)$, and $W(0.1)$. We now define

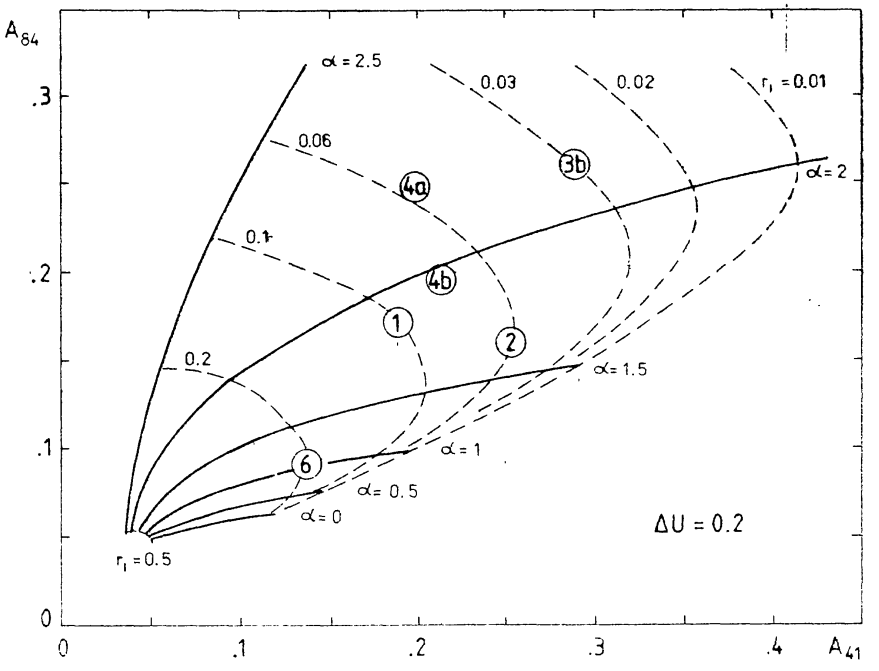

Fig. 6. The A_{84} - A_{41} diagram (cf. Section 3.3). Circled numbers correspond to observed profiles listed in Table 1. The accuracy of their A_{84} and A_{41} values is roughly ± 0.05.

$$A_{84} = \log u(0.4) - \log u(0.8) = \log W(0.4) - \log W(0.8), \quad (9a)$$

$$A_{41} = \log u(0.1) - \log u(0.4) = \log W(0.1) - \log W(0.4). \quad (9b)$$

These two parameters turn out to depend primarily on α and r_1, their dependence on Δu being much weaker. This can be seen from Figs. 6 and 7. In practical applications it is therefore sufficient to have a crude estimate of Δu to enter the appropriate $A_{84} - A_{41}$ diagram and to find α and r_1

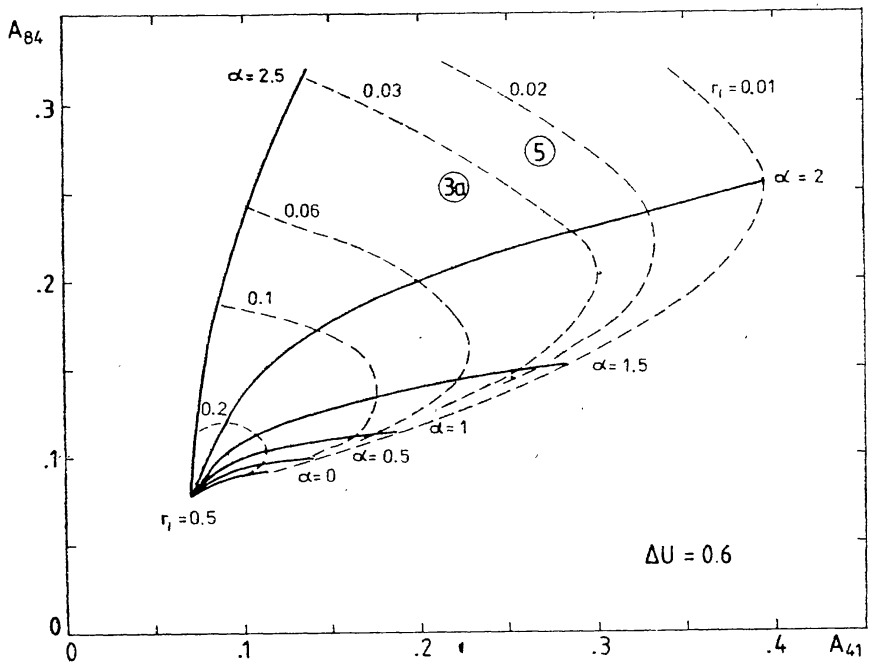

Fig. 7. Same as in Fig.6, but for $\Delta u = 0.6$.

The observed half-width at a specific intensity level can also be used to determine the true value of $V_d \sin i$. This may be particularly useful in the case of profiles without well defined peaks. For example, if $W(0.8)$ is expressed in km/s then

$$(V_d \sin i)_{\text{true}} = W(0.8)/u(0.8). \quad (10)$$

The dimensionless half-width $u(0.8)$ is a function of α, r_1, and Δu. With a reasonable accuracy we can represent this dependence by

$$\log u(0.8) = \delta_1(\alpha, r_1) + \delta_2(\Delta u), \quad (11)$$

where δ_1 is almost independent of Δu (cf. Fig. 8). Thus with α and r_1 determined from the $A_{84} - A_{41}$ diagram we can use Eq. (11) and Fig. (8) to determine $u(0.8)$.

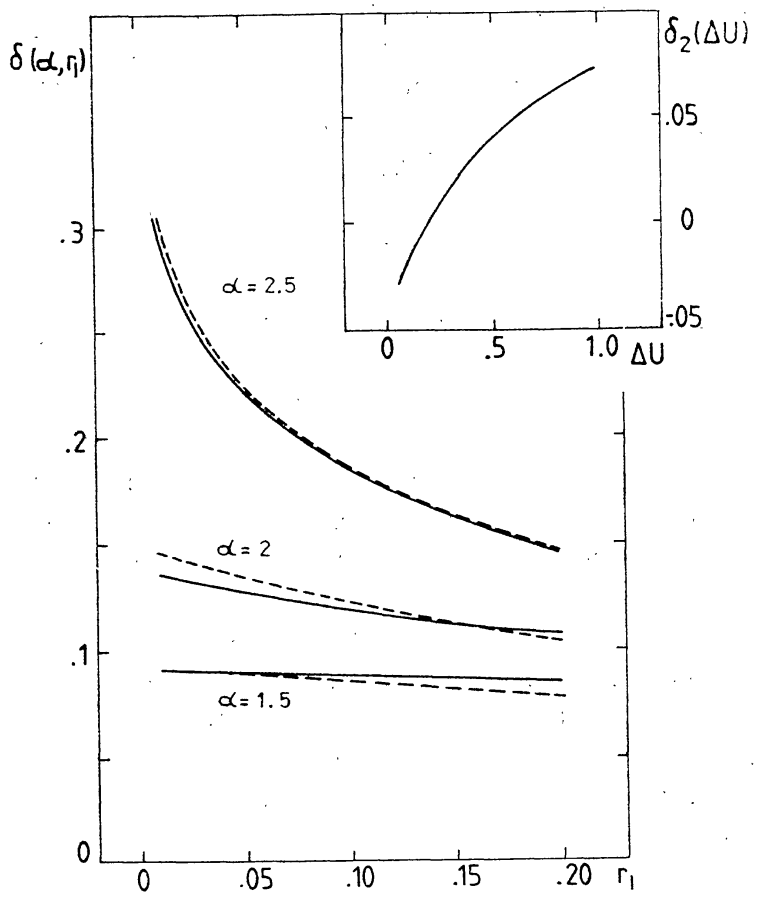

Fig. 8. The δ_1 and δ_2 functions. Solid lines for $\Delta u = 0.2$, broken lines for $\Delta u = 0.6$. Cf. Section 3.3.

4. Interpretation of the Observed Profiles

4.1. The Visibility of the Peaks.

It has been established from observational evidence that the visibility of double lines usually indicates a high orbital inclination and vice-versa. The results of Sections 3.1 and 3.2 may suggest that an important factor here is the spectral resolution. Indeed, let us consider, for example, the Kraft's (1962, 1964) survey of cataclysmic variables. With the dispersion of 180 Å/mm, used for the majority of objects, the spectral resolution was roughly $\Delta v = 300$ km/s. The typical values of $V_d \sin i$ for systems with $i > 60°$ were 400 —700 km/s. Thus we find that $\Delta u = \Delta v / V_d \sin i = 0.5$ for high orbital inclinations, $= 1$ for $i = 30$-$45°$, and $= 2$ for $i = 15$-$20°$. Therefore the effect of spectral resolution must have been crucial in preventing the detection of double lines at lower orbital inclinations.

The situation, however, appears more complicated. First, we have examples where the spectral resolution is sufficient to show the double structure, yet the doubling is not detectable or seen only occasionally (e.g. in SS Cyg, cf. Section 4.3). We also note cases with doubling present, but with the central intensity $F(0)$ much higher than expected from the theory. A good example here is DQ Her (Hutchings *et al.* 1979, Fig. 1) in which Hβ and Hγ are clearly double but their central depressions are less pronounced than in higher Balmer lines and in theoretical profiles; at the same time the HeIIλ 4686 line is only marginally double.

Considering effects likely to affect the shape of an emission line, we note that the phase-averaged effect of the S-wave component will rather make the peaks more pronounced. The absorption lines (Mayo *et al.* 1980) will make the central depression deeper, as seen — for example — in WZ Sge or Z Cha. In the case of inclinations close to 90° the effect of a high optical thickness is likely to decrease the intensity of the peaks, but such an effect should certainly be negligible at low inclinations. Thus the most general alternative is to postulate the presence of an extra, low-velocity emission filling-in the central parts of the double line. This could come from the material on the disk's outer edge of finite z-thickness, not included in our flat-disk models. It could also come from material in the immediate vicinity of the central star provided it is no longer in the Keplerian rotation.

4.2. Determination of a and r_1.

Table 1 lists examples of observed profiles. The Δu values have been roughly estimated from the available data, while the half-widths W have been determined from the published profiles; it should be emphasized that in some cases the accuracy of our determinations is necessarily rather low. All the examples are shown in Fig. 6 or 7 with their appropriate A_{84} and A_{41} values. From these diagrams we now find a and r_1. Finally, using the procedure outlined in Section 3.3 we determine $V_d \sin i$. The results contained in Table 1 can be summarized as follows:

(i) except for G61-29, we find that the values of a are in the range 1.7-2.2, while the values of r_1 are $\leqslant 0.1$;

(ii) the resulting values of $V_d \sin i$ are in a reasonable agreement with those determined directly from the peaks;

(iii) in the case of SS Cyg the two sets of data lead to almost identical results (for further discussion see Section 4.3); in the case of DQ Her we note that the parameters obtained from Hβ are somewhat different from those obtained from the HeII λ 4686 line.

Table 1

Analysis of the Observed Emission Profiles

		Δu	$W(0.8)$ $W(0.4)$ $W(0.1)$	A_{84} A_{41}	α	r_1	$V_d \sin i$
1	HT Cas, Hβ, Hγ, Hδ Young *et. al.* (1981)	0.2	950 1400 2150	0.17 0.19	1.8	0.10	740
2	Z Cha, Hβ Fabian *et al.* (1979)	0.2	935 1350 2400	0.16 0.25	1.7	0.06	740
3a	SS Cyg, Hβ Stover *et al.* (1980)	0.6	350 620 1040	0.25 0.22	2.2	0.04	210
3b	SS Cyg, Hβ, Hδ Cowley *et al.* (1980)	0.2	350 630 1220	0.26 0.29	2.1	0.03	240
4a	DQ Her, Hβ Hutchings *et al.* (1979)	0.2	430 770 1230	0.25 0.20	2.2	0.05_5	300
4b	DQ Her, HeII λ 4686 Hutchings *et. al.* (1979)	0.2	580 900 1440	0.19 0.20	1.9	0.08	450
5	Stepanyan's star, Hβ, Hγ Young and Schneider (1981)	0.6	400 750 1400	0.27 0.27	2.2	0.02_5	240
6	G61-29, HeI λ 3888 Smak (1975)	0.2	825 1020 1420	0.09 0.14	1.0	0.20	700

With respect to the values of α and r_1 it is necessary to emphasize that they could be taken literally only in the case when the $r^{-\alpha}$ dependence applies to the entire disk. In general, the r_1 value determined within our procedure is likely to be only an upper limit to the inner radius of the disk (of. Section 4.3).

4.3 Direct Determination of $f(r)$.

In the case when the profile is determined in detail by the observational data it is possible to deconvolve it and to obtain $f(r)$ directly. In order to verify the significance of parameters found in the previous section we now perform such a direct analysis for two examples: the Hβ line in SS Cyg

(Stover *et al.* 1980, Fig. 5) and the HeI λ 3888 line in G61-29 (Smak 1975, Fig. 3). The results are shown in Fig. 9.

In the case of SS Cyg we find that over a wide range of radii we indeed have $f(r) \sim r^{-\alpha}$, with $\alpha = 2.2$, as listed in Table 1. We note also that for radii comparable and smaller than r_1 (as listed in Table 1) the $f(r)$ curve begins to deviate from the $r^{-\alpha}$ line. It appears therefore that r_1 would

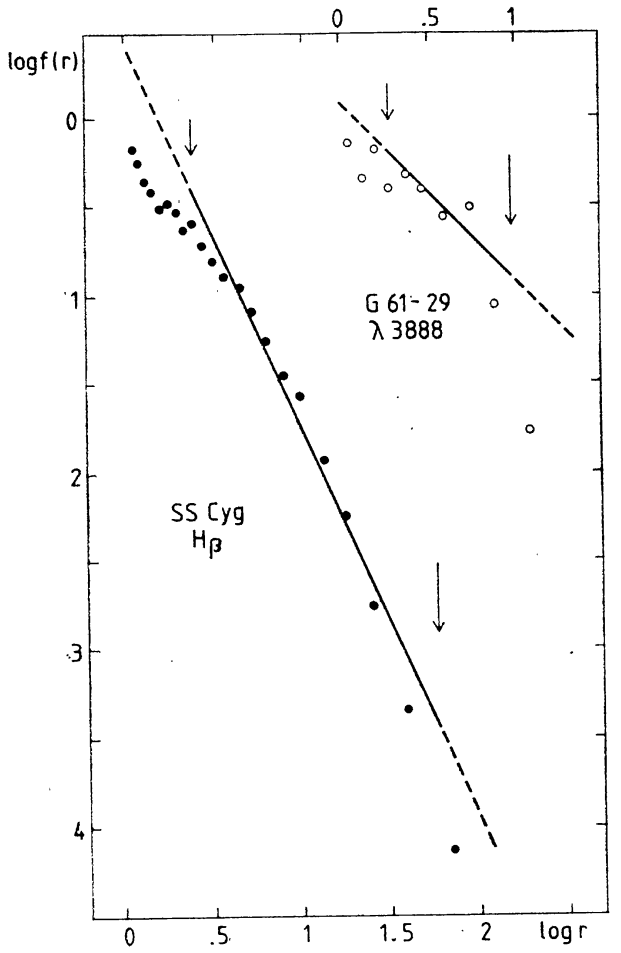

Fig. 9. The emissivity versus radius, as obtained directly from the observed profiles. The zero point of $\log f(r)$ is arbitrary. The zero point of $\log r$ corresponds to outermost point in the wing of the observed profile. The long arrows correspond to $V_d \sin i$, while the short arrows — to r_1 (as listed in Table 1). The slopes of the lines are those listed as α in Table 1.

represent the true inner radius of the disk only in the case of strict applicability of the $r^{-\alpha}$ law. In a real situation r_1 only indicates the radius at which the $r^{-\alpha}$ approximation breaks down and is larger than the true inner radius. In the case considered we find (from Fig. 9, or directly from the extension of the wings) that $r_{1,true} \approx 0.015$. Turning to the outer edge of the disk we note from Fig. 9 that — again — the $r^{-\alpha}$ approximation appears to break down at the outer edge as defined by $V_d \sin i = 210$ km/s (Table 1). The $f(r)$ function obtained from the deconvolution procedure clearly extends beyond that radius. This is a direct consequence of the fact that the line is not double. Alternatively, if we stop the deconvolu-

tion procedure at the radius corresponding to $V_d \sin i = 210$ km/s we end with a residual profile, representing extra emission responsible for the obliteration of the double structure. The width of this residual profile corresponds — obviously — to the adopted value of $V_d \sin i$, while its central intensity amounts to about one third of the original profile. At this point it is worth to note that line doubling has been seen in SS Cyg at least on two occassions: in the CaII lines by Walker and Chincarini (1968) and in the Balmer lines by Giovannelli (1981). In both cases the separation of the peaks was roughly 2×200 km/s in agreement with $V_d \sin i = 210$ km/s found here. From this evidence we have to conclude that the extra emission in SS Cyg is a variable phenomenon.

In the case of G61-29 we note from Fig. 9 that the radial extension of the disk is rather small: r_1 in Table 1 is 0.2, while the maximum extension of the wings implies an inner radius of about 0.1. Under such circumstances the range of applicability of the r^{-a} law is rather narrow. What we note in contrast to SS Cyg is the sharp drop in $f(r)$ at the outer radius defined by the observed value of $V_d \sin i$. In spite of that, however, G61-29 is similar to SS Cyg: in addition to the double lines we observe an extra single component. It is sufficiently narrow (in the λ 3888 line, but not in other lines; cf. Smak 1975) not to obliterate the double structure. And, curiously enough, it is slightly red shifted.

5. Concluding Remarks

One of the most important results of the present paper is that the emission line profiles in typical cataclysmic variables can be represented with the emissivity law $f(r) \sim r^{-a}$, where $a \cong 2$, and the emission extends down to inner radii as small as 0.02-0.10 of the outer radii. There appears to be no systematic difference between objects representing different types of the cataclysmic variables. This should be compared and contrasted with the evidence available concerning the distribution of the continuous radiation. In the case of two dwarf novae: U Gem (Smak 1971) and Z Cha (Smak 1979) it was found that the surface brigthness of the disk is higher in its outer regions. On the other hand, in the case of nova DQ Her (Dmitrienko and Cherepashchuk 1980) the surface brightness appears to increase toward the center of the disk. It appears that the continuous radiation is primarily a function of the accretion regime. The emission lines, with their r^{-2} dependence, seem to be related to the luminosity and/or surface temperature of the central star.

In conclusion, it is a pleasure to thank Dr. F. Giovannelli for useful discussions on SS Cyg. It is also a pleasant duty to acknowledge that all

the calculations were made on the PDP 11/45 computer donated to the Copernicus Astronomical Center by the U.S. National Academy of Sciences on the initiative and through the action of Dr. C. R. O'Dell and Mr. A. M. Baer.

REFERENCES

Cowley, A.P., Crampton, D., and Hutchings, J.B. 1980 *Ap. J.*, **241**, 269.
Dmitrienko, E.S. and Cherepashchuk, A.M. 1980 *Astr. Zh.*, **57**, 749.
Fabian, A.C., Pringle, J.E., Whelan, J.A.J., and Bailey, J.A. 1979 *IAU Coll. No. 46*, eds. F. M. Bateson *et al.* (Hamilton, N.Z.: University of Waikato Press), p.65.
Giovannelli, F. 1981 Private information.
Huang, S.-S. 1972 *Ap. J.*, **171**, 549.
Hutchings, J.B., Cowley, A.P., and Crampton, D. 1979 *Ap. J.*, **232**, 500.
Kraft, R.P. 1962 *Ap. J.*, **135**, 408.
— 1964 *Ap. J.*, **139**, 457.
Mayo, S.K., Wickramasinghe, D.T., and Whelan, J.A.J. 1980 *M.N.R.A.S.*, **193**, 793.
Smak, J. 1969 *Acta Astr.*, **19**, 155.
— 1971 *ibid*, **21**, 15.
— 1975 *ibid*, **25**, 227.
— 1979 *ibid*, **29**, 309.
— 1981 *ibid*, **31**, No. 1.
Stover, R.J., Robinson, E.L., Nather, R.E., and Montemayor, T.J. 1980 *Ap. J.*, **240**, 597.
Walker, M.F. and Chincarini, G. 1968 *Ap. J.*, **154**, 157.
Williams, R.E. 1980 *Ap.J.* **235**, 939.
Young, P. and Schneider, D.P. 1980 *Ap.J.*, **238**, 955.
— 1981 *Ap. J.*, in press.
Young, P., Schneider, D.P., and Shectman, S.A. 1981 *Ap.J.*, **245**, 1035.

Note added in proof: Stover (*Ap. J.*, **248**, 684, 1981) published recently new, high resolution spectroscopic observations of U Gem. From his Hβ profiles, using the method described in Sections 3.3 and 4.2, we find: $a = 1.5$ and $r_1 \sim 0.03$, in perfect agreement with values given in his Section IIIf.